

Tunneling through Al/AIO_x/Al junction: analytical models and first principles simulations

M. Zemanová Diešková,¹ A. Ferretti,^{2,3} and P. Bokes^{1,3,*}

¹*Department of Physics, Faculty of Electrical Engineering and Information Technology,
Slovak University of Technology, Ilkovičova 3, 812 19 Bratislava, Slovak Republic*

²*Centro S3, CNR-Istituto Nanoscienze, I-41125 Modena, Italy.*

³*European Theoretical Spectroscopy Facility (ETSF, www.etsf.eu)*

(Dated: January 29, 2013)

We study from first principles the transport properties of Al/AIO_x/Al tunnel junctions. On this basis, we analyze the reliability of two analytical models for the conductance, namely the trapezoid potential barrier model and a tight-binding model. Our findings show that (i) the interface width used in the models is determined by the electronic density profile, and it is shorter than the width one expects from the atomic arrangements; (ii) the effective mass, found to be about on third of the free electron mass, can be determined from the oxide band-structure calculations, and (iii) the barrier height is given by one fourth of the bandgap in the oxide, which explains the apparently small values found for these junctions experimentally.

PACS numbers: 73.40.Rw; 73.40.Gk; 71.15.-m

I. INTRODUCTION

Tunneling of electrons through aluminum-aluminum oxide (Al/AIO_x/Al) junctions is one of the prototypical examples of quantum-mechanical tunneling in solid state physics. Fisher and Giaever in their pioneering work¹ demonstrated the tunneling character of the transport of electrons through this interface and by comparing their results with the predictions of Holm² for tunneling through vacuum gap, they initiated the interpretation of tunneling measurements through thin metal-insulator-metal junctions using potential barrier model. The minimal form of this model contains two parameters - the barrier width d , which indicates the physical width of the oxide, and its height W , given by the energy difference between the Fermi energy and the bottom of the conduction band in the oxide. In practice, several other parameters enter the model³⁻⁵: the electron's effective mass in the oxide or the dielectric constant of the oxide used within an additional image-charge potential. Further parameters are used for fine-tuning the shape of the barrier, e.g. its asymmetry⁵. Clearly, having a large set of parameters, it is no surprise that the simple barrier model can be fitted to the experimental current-voltage characteristics well⁶⁻⁹, but at the same time, it rises questions about the relevance of the model itself.^{10,11} For example, the inclusion of the image potential can have a significant effect on the effective barrier width, but its presence depends on the time scales of the tunneling electrons and the interface plasmons in the metal^{12,13}.

On the other hand, much more detailed and parameter-free models of the interface can be constructed using first principles calculations¹⁴⁻¹⁹ even though the size of the modeled interfaces is somewhat restricted due to the numerical cost of these calculations. Nevertheless, in many experiments^{8,9,11,15,20-22} the studied interfaces have widths within the reach of *ab initio* simulations so that the accuracy of the potential barrier model to the interpretation of tunneling data can be tested. Specifically, Jung *et al*¹⁵ presented such a study comparing the character of the equilibrium projected density of states of the Al/AIO_x/Al interface obtained by a first principles simulation with the potential barrier model. They found

that the parameters of the potential barrier model fitted to the experimental data are in qualitative agreement with the parameters of the first principles calculations. The potential barrier model included the image potential and hence also the dielectric constant which effectively narrowed and lowered the potential barrier.

In this work we test the performance of the potential barrier model by comparing the predicted conductance to *ab initio* calculations²³⁻²⁵. We test this for Al/AIO_x/Al junctions of four different widths d and show that it is essential to use an effective mass in the oxide and an effectively shorter width of the tunneling region within the potential barrier model. We also present an analytical tight-binding model for the conductance that describes the *ab initio* results more accurately than the potential barrier model. The parameters of the latter are extracted from the ground state *ab initio* calculations of the junction. In Sec. II and III we introduce the analytical details of the models. The *ab initio* results for ground state properties of the studied junctions are presented in Sec. IV and V, together with the computational parameters used in the calculations. Finally in Sec. VI we compare the conductances obtained using the *ab initio* calculations and the conductances obtained from the analytical models.

II. POTENTIAL BARRIER MODELS OF THE INTERFACE

The starting assumption of the potential barrier model is that inside the metallic electrodes, on the left and right of the insulator, the electrons behave like free quasi-particles with their energy being in a separable form⁵²

$$E = E_z + E_{\parallel} = k_z^2/2 + k_{\parallel}^2/2 \quad (1)$$

where k_z is the component of electron's momentum perpendicular to the interface and k_{\parallel} the component of momentum parallel to the interface. The current density, induced by an infinitesimal bias voltage, consists of a sum of contributions from the electrons occupying states in the energy window around the Fermi energy E_F , with their momentum

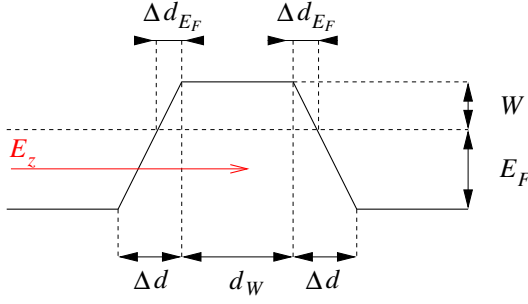


FIG. 1: (Color online) The trapezoid potential barrier used to model ultra-thin AlO_x interface.

opposite to the drop of the bias voltage ($k_z > 0$). Hence, the conductance per area is given by the expression⁵³

$$g = 2 \int \frac{d^2 k_{\parallel}}{(2\pi)^2} \int_{-\infty}^{\infty} \frac{dE_z}{2\pi} \delta(E_F - E_z - E_{\parallel}) T(E_z), \quad (2)$$

$$= \int_0^{\infty} \frac{dE_{\parallel}}{2\pi^2} T(E_F - E_{\parallel}), \quad (3)$$

where $T(E_z)$ is the transmission function, the probability for an electron to pass through the junction, and E_F is the Fermi energy.

The simplest expression for the transmission $T(E_z)$ is based on a metal-vacuum-metal interface³⁻⁵, where the barrier height W is given by the potential energy in the vacuum with respect to the Fermi energy of the metal.

In Sec. VI we will demonstrate that there are two essential features of the potential barrier models that need to be taken into account for the description of ultra-thin interfaces: (1) the barrier needs to have transition regions between the metal and the insulator of width Δd , where the potential energy changes continuously, (2) the effective mass of the electrons in the insulator needs to be accounted for. These two requirements can be fulfilled by using a specific shape of the potential barrier. In this work we use a trapezoid potential barrier (TB) as defined in Fig. 1.

On the other hand, in Sec. VI we will also demonstrate that approximate expressions for the transmission as well as for the energy integration in Eq. (3) are sufficient for an accurate evaluation of the model conductance. For the trapezoid potential barrier, the WKB approximation for the transmission gives

$$T(E - E_{\parallel}) = \exp\{-F(E - E_{\parallel})\}, \quad (4)$$

$$F(E - E_{\parallel}) = 2 \int_{-d(E_{\parallel})}^{d(E_{\parallel})} \sqrt{2m_{\text{eff}}[W(z) + E_{\parallel}]} dz, \quad (5)$$

where m_{eff} is the effective mass of the electrons in the insulator, $-d(E_{\parallel})$ and $d(E_{\parallel})$ give the region where $[W(z) + E_{\parallel}] \geq 0$, and $W(z)$ is the trapezoid potential profile. Accounting only for the largest contribution from the states close to the Fermi energy in the integral in Eq. (3), $E_{\parallel} \sim E_F$, we obtain the

following simple analytical expression:

$$g \approx -\frac{e^{-F(E_F)}}{2\pi^2 F'(E_F)}, \quad (6)$$

where

$$F(E_F) = 2\sqrt{2m_{\text{eff}}W} \left(d_W + \frac{2}{3}\Delta d E_F \right), \quad (7)$$

$$F'(E_F) = -\frac{2}{\sqrt{2m_{\text{eff}}W}} (d_W + 2\Delta d E_F). \quad (8)$$

We will refer to Eq. (6) as the $\text{TB}^{A,m_{\text{eff}}}$ model (A stands for “analytical” as compared to the numerically calculated transmission for the trapezoid potential barrier - TB^N). We note that the introduction of two transition regions of width Δd adds to the exponent of the transmission amplitude only a small fraction of Δd , namely $(2/3)\Delta d E_F$. This results in a substantial increase of the conductance which is needed for the agreement of the TB model and *ab initio* results (see Sec. VI).

III. ATOMIC sp MODEL OF THE INSULATOR

It is typically assumed that the barrier height in the potential barrier model corresponds to energy distance between the Fermi energy and the closest among the valence or conduction bands of the insulator, or even to its whole bandgap. However, fits of the potential barrier model to experimental data often lead to unphysically small values if one follows this interpretation. Various arguments like interface roughness¹⁰ or image potential⁴ have been suggested to correct for this underestimation, but perhaps the most important one – the principal difference in the energetic spectrum of the real insulator and the vacuum gap – received less attention^{3,26}.

To account for a more realistic electronic structure of the insulator we consider a minimal tight-binding model of a sp -like insulator with rock-salt crystal structure. For our purposes, the cation with s -like orbital plays the role of aluminum and the anion with p -like orbital the oxygen atom. While this is different from the true structure of alumina, this model works surprisingly well even for the disordered aluminum oxide found in our interfaces, as will be shown in Sec. IV.

The sp model has four parameters: the onsite atomic energies of the cation (ϵ_s) and anion (ϵ_p), the hopping matrix element between the two atoms (t), and the length of the edge of the conventional unit cell (cube) a . A standard calculation leads to valence (v) and conduction (c) band energies

$$E_{c/v}(\mathbf{k}) = E_F \pm \frac{E_g}{2} \sqrt{1 + \frac{8m_{\text{eff}}^{-1}}{E_g a^2} \sum_{i=1}^3 \sin^2(k_i a/2)} \quad (9)$$

where $m_{\text{eff}} = E_g/(2t^2 a^2)$ is the effective mass of the electrons close to the conduction band minimum, equal in magnitude that of the valence band maximum. The two bands are separated by the bandgap $E_g = \epsilon_p - \epsilon_s$, and the energy in the middle of the gap is

$$E_F^{\infty} = \frac{\epsilon_p + \epsilon_s}{2}. \quad (10)$$

In the tunneling regime, the current is carried by the electronic states in the bandgap,^{27–29} i.e. the evanescent Bloch states with imaginary wavenumber $k_z = i\kappa$:

$$\phi_{\kappa,k_{\parallel}}(\mathbf{r}) \sim e^{-\kappa z} e^{i\mathbf{k}_{\parallel} \cdot \mathbf{r}} u_{\kappa,k_{\parallel}}(\mathbf{r}). \quad (11)$$

The WKB-like result for the transmission takes then the form

$$T_{k_{\parallel}}^{sp}(E) \sim |\phi_{\kappa,k_{\parallel}}(\mathbf{d})|^2 \sim e^{-2\kappa(E,k_{\parallel})d}, \quad (12)$$

where \mathbf{d} is a vector normal to the interface with the length given by the width of the interface ($|\mathbf{d}| \sim d$). $\kappa(E, k_{\parallel})$ can be obtained from Eq. (9) using the substitution $k_z = i\kappa$ therein. The transmission can be then used in the calculation of the conductance in Eq. 2. The largest contributions to the conductance come only from $\kappa a/2 < 1$, $k_{\parallel} a/2 < 1$, so that the $\sin(\cdot)$ functions in the dispersion can be expanded in Taylor series. Keeping only the first two terms we find⁵⁴

$$\kappa(E, k_{\parallel}) = \sqrt{v(E)m_{\text{eff}}E_g/2 + k_x^2 + k_y^2}, \quad (13)$$

$$= \sqrt{2[v(E)m_{\text{eff}}E_g/4 + E_{\parallel}]}, \quad (14)$$

where we have introduced a multiplicative factor $v(E)$ accounting for the relative distance of the energy E from the middle of the gap,

$$v(E) = 1 - 4 \left(\frac{E - E_F^{\infty}}{E_g} \right)^2, \quad (15)$$

which is close to 1 for $E \sim E_F$. We note that by using the Taylor expansion the model becomes independent of the size of the conventional cell a . The transmission $T_{k_{\parallel}}^{sp}(E)$ is similar to the WKB result for a potential barrier [Eqs. (4-5) for a constant barrier height W]. Hence, making the same approximations as in Sec. II and substituting $W \rightarrow v(E_F)E_g/4$ we find an analytical expression for the transmission through a sp insulator of width d precisely of the form of Eq. (6), where

$$F_{sp}(E_F) = 2\sqrt{v(E_F)m_{\text{eff}}E_g/2}d, \quad (16)$$

$$F'_{sp}(E_F) = -\frac{2}{\sqrt{v(E_F)m_{\text{eff}}E_g/2}}d. \quad (17)$$

This represents one of the main results of our paper: the potential barrier height W is related to the bandgap through the relation $W = v(E_F)E_g/4$. Since the Fermi energy in our junctions is close to the center of the gap (Sec. IV) where we have $v(E_F) \sim 1$, we expect that the bandgap is about four times larger than the barrier height obtained from the fits to the experimental data. This explains the typical situation in Al/AIO_x/Al junctions where W can be as small as 2eV or less, which is to be compared with the bandgap of alumina being about 7–9eV. Further comparisons will be made in the Sec. VI where the sp model is compared to the *ab initio* calculation of the conductance.

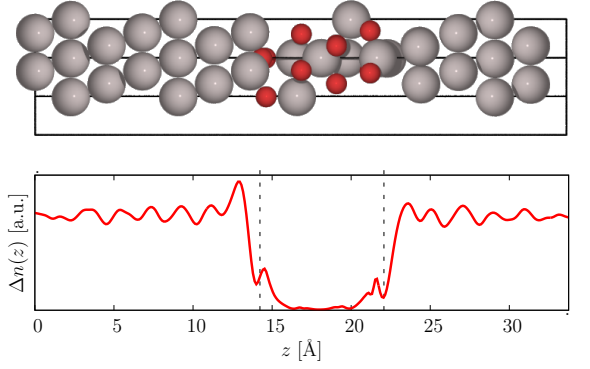


FIG. 2: (Color online) The 4L structure (above) and the corresponding averaged electronic density of the occupied transmitting states. The dashed lines indicate the positions of the metal-oxide boundary obtained according to Eq. (18).

IV. FIRST PRINCIPLES CALCULATIONS OF THE AL/AIO_x/AL INTERFACES

The Al/AIO_x thin film is well known for its difficulties to be grown in an ordered form^{30,31}. The process of oxidation consists of a quick chemisorption of oxygen on a clean Al surface which is followed by a complex diffusion process leading to various widths of the interface which is typically disordered^{22,32–34}. The model that we consider is on the other hand relatively simple and ordered. We followed Jennison^{35,36} at constructing chemisorbed layer of oxygen on an ideal Al(111) $\sqrt{3} \times \sqrt{3}$ surface (three Al atoms per layer), modelled as a slab 6 layers thick (left electrode). Next we were adding Al and O atoms and relaxed the geometry until we found a stable interface having two layers of oxygen atoms (2L). Finally we enclosed the interface with four ideal Al(111) layers (right electrode) and connected it with the left electrode through periodic boundary conditions. Performing this procedure two different geometries of the interfaces were identified: (1) an asymmetric structure, corresponding to the ultra-thin AlO_x layer investigated by Jennison, and (2) a symmetric structure which did not contain the layer of chemisorbed oxygen next to the bottom Al electrode. More details on the differences between the asymmetric and symmetric structures can be found elsewhere³⁷; in our present work we will consider only structures derived from the asymmetric geometry.

Motivated by the geometry of the asymmetric 2L interface model we have constructed thicker Al/AIO_x/Al by adding one (3L), two (4L) or three (5L) full oxygen layers sandwiched between monoatomic (Al1) or diatomic (Al2) layers of aluminum. The resulting geometries were optimized until the forces on the atoms were smaller than 0.002 Ha/a_B, while the Al atoms beyond the first layer of bulk metal were kept fixed. An example of the resulting geometric structure of 4L is shown in Fig. 2. We should mention that these models are not necessarily the only ones possible for the interface of the concerned width. Due to the above described tendency of AlO_x systems towards disorder, we expect that many different vari-

System	d [Å]	E_g [eV]	ΔE_F [eV]	$v(E_F)$
2L	4.5	7.0	1.5	0.82
3L	5.5	6.5	-0.25	0.99
4L	7.8	6.5	-1.0	0.91
5L	9.8	6.5	-1.0	0.91

TABLE I: Values of the interface widths, band-gaps, Fermi energy shifts and the shift factor $v(E_F)$ obtained from *ab initio* calculations.

ations could be found with larger surface cells. The structures identified here need to be taken as few samples of the great variety of possible geometrical arrangements. However, the comparison of the projected density of states (PDOS) for symmetric and asymmetric 2L junctions (see Ref. [37]) suggests that these differences lead to small changes in their conductances.

All of the ground state properties and optimizations were done using the Quantum Espresso distribution³⁸. We have employed the PBE exchange-correlation functional, atomic cores were described using ultra-soft pseudopotentials resulting in well converged electronic structure close to the Fermi energy, using a cutoff energy of 12.5 (125) Ha for wavefunctions (charge density). Due to the large size of the supercell, a $6 \times 6 \times 1$ Monkhorst-Pack k-point grid was sufficient to converge the total energy and the electronic density.

In Fig. 2, in parallel with the geometric structure of the 4L interface, we show the profile of the plane-averaged electronic density of the scattering states $\Delta n(z)$ (e.g. localized states on oxygen atoms are not included). We see that the rapid drop and increase in the density appears at the boundary between the metal and the oxide. We use $\Delta n(z)$ as the quantity for the determination of the interface width from our *ab initio* calculations, in close analogy with the determination of the position of surfaces at metal-vacuum interfaces³⁹; for the left boundary we use

$$z_L = \int_{-\infty}^{z_I} z \frac{d\Delta n(z)}{dz} dz / \int_{-\infty}^{z_I} \frac{d\Delta n(z)}{dz} dz, \quad (18)$$

where z_I is a position in the center of the insulator. Similar expression is used for the determination of the right boundary z_R which together with z_L give the estimate of the interface width $d = z_R - z_L$ used within our potential barrier and *sp* models in Sec. VI. The resulting interface widths are given in the Table I. In the following we will also refer to the width of the transition region between the metal and the oxide, which can be estimated from the averaged density to be $\Delta n \approx 2.0 \text{ Å}$. This value will be used for the determination of the width of the transition region in the potential barrier model (Fig. 1).

We note that for the calculation of the positions $z_{L/R}$ we do not necessarily need to use the density $\Delta n(z)$ obtained from the scattering states in the transport calculations (see Sec VI), but is it equally good to use the partial density of the states close to the Fermi energy that can be obtained from any ground state code (e.g. Quantum Espresso). On the other hand, the total electronic density or the Kohn-Sham potential

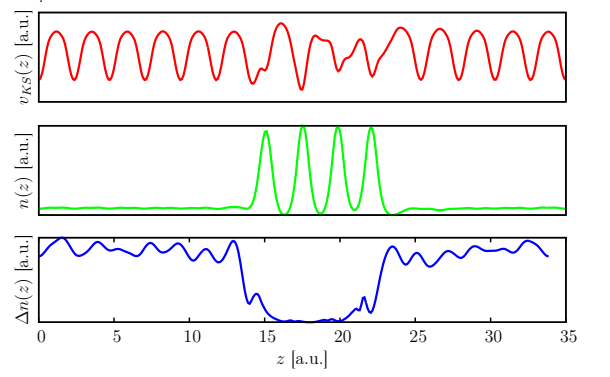


FIG. 3: (Color online) The comparison of the average Kohn-Sham potential $v_{KS}(x)$, the total density $n(z)$ and the contribution to the density from the states close to the Fermi energy $\Delta n(z)$. Clearly, the latter can be unambiguously used for the definition of the width of the interface using the Eq. 18.

(which is frequently but incorrectly believed to be the origin of the potential barrier in the model from Sec. II) are not suitable for this calculation, as it is clearly demonstrated in Fig. 3.

The second important parameter of the potential barrier and the atomic *sp* models is the insulator band gap E_g . It can be extracted from the projected density of states (PDOS), where the Kohn-Sham eigenstates of the interface are projected on atomic orbitals. Figure 4 shows the PDOS for the 4L interface, where the PDOS of atoms in each layer are added together, green lines corresponding to the Al layers and the red lines to the oxygen layers. The oxide bandgap is estimated as the energy distance between the onset of the valence bands on the oxygen atoms below the Fermi energy, and the onset of the mixed Al and O bands above the Fermi energy. From the PDOS we can also obtain the energy distance between the midgap energy and the Fermi energy, ΔE_F , needed for the *sp* model. The calculated bandgaps and ΔE_F for all studied interfaces are collected in the Table I. Interestingly, in spite of the well known bandgap problem of the DFT^{40–42}, these bandgaps appear to be in very good agreement with recent experimental results for the Al/Al₂O₃ interfaces^{43,44} which found $E_g = 6.4 \text{ eV}$.

While the bandgap stays roughly the same for all of the studied interfaces 2L – 5L, the Fermi energy shifts with respect to the middle of the gap from positive (conventionally called the electron tunneling regime) to negative values (hole tunneling). However, the factor $v(E_F)$ stays close to one in all the cases (see Table I), as anticipated already in Sec II. The energy difference between the bottom of the conduction band and the Fermi energy determined experimentally⁴³ was found to be $E_c - E_F = 2.9 \pm 0.2 \text{ eV}$ which is 1 eV smaller than the DFT value found here for 4L and 5L, but on the other hand, in good agreement with 2L and 3L, which perhaps indicates larger sensitivity of this quantity on the particular system.

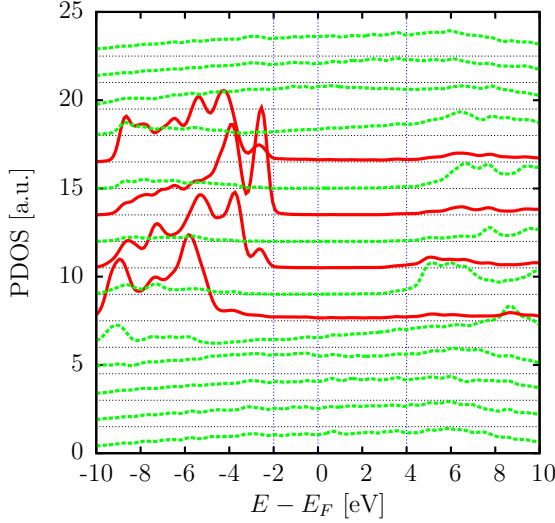


FIG. 4: (Color online) The projected density of states for the AlOx 4L interface. The distance of the valence band to the Fermi energy, being less than half the distance to the conduction band, is taken as the effective barrier height.

V. ELECTRONIC STRUCTURE OF AN IDEAL INSULATOR

The potential barrier model as well as the *sp* model also rely on the knowledge of the effective mass m_{eff} of the electrons in the insulator or barrier region. To calculate it we have considered a first principles model of the insulator extracted from the geometry of the 4L junction. Namely, it consists of a supercell of length $l = 8.11 a_B$ in the z direction and with identical dimensions in the two remaining in-plane directions [i.e. $\sqrt{3} \times \sqrt{3}$ Al(111)]. The supercell contains two layers of oxygen and two layers of 2/3 filled Al planes. (the 3rd and 4th oxygen layers in Fig. 2 from the left and their immediately following Al layers respectively). This way, the chemical composition actually corresponds to alumina, Al_2O_3 .

The DFT ground state calculation has been done with the same specifications as for the full interface (Sec. IV) except for the k -point grid being here $6 \times 6 \times 6$ due to smaller extent in the z direction. The following band-structure calculation has been done using the PWCOND program²³ that is capable of obtaining the so called complex band-structure, i.e. energy bands for imaginary as well as real Bloch k -vectors. We have checked that calculations of the band-structure for real k -vectors using the Quantum Espresso and the PWCOND gave identical results so that the parameters involved in the PWCOND program were correctly chosen.

The band-structure along the direction normal to the interface (z) is shown in Fig. 5. First of all we note that the bandgap obtained here, $E_g^\infty \sim 4\text{eV}$ (in agreement with the previous DFT-PBE results for bulk $\gamma\text{-Al}_2\text{O}_3$ ^{45,46}), is significantly smaller than the bandgap extracted from the PDOS of the full junction ($\sim 6.5\text{eV}$). Interestingly, the experimental value of this phase of alumina is $E_g^{\text{exp}} = 7\text{eV}$, which can be obtained

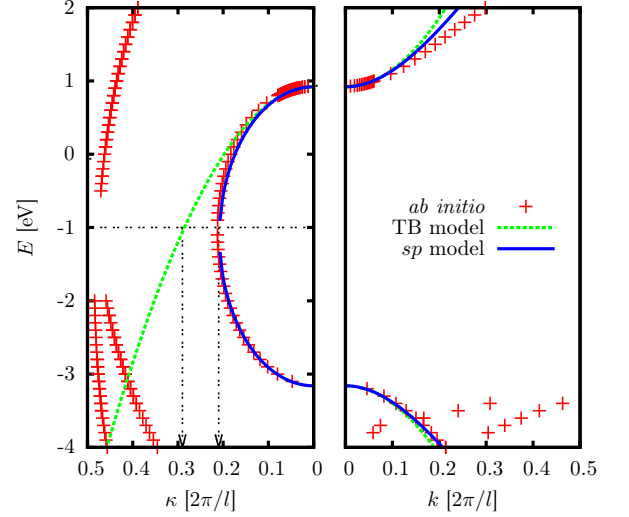


FIG. 5: (Color online) The imaginary (left) and real (right) band structures from *ab initio* calculations compared with the band-structures of the *sp* and potential barrier models. The *sp* model gives an excellent fit for both real and imaginary band-structure for $m_{\text{eff}} = 0.35$ and $E_g = 4.0\text{eV}$.

also computationally if the DFT-PBE result is followed by a GW calculation⁴⁶.

The DFT band structure in Fig. 5 is fitted with two model dispersions. The TB model uses a free-electron like dispersion $E_c(k) = \epsilon_c + k^2/(2m_{\text{eff}})$ which after fitting gives the effective mass $m_{\text{eff}} = 0.35$. The atomic *sp* model [Eq. (9)] in the approximation $ka/2 < 1$, which is used in the analytic expression for the conductance, gives (for $k_x = k_y = 0$) the dispersion:

$$E_{c/v}(k) = E_F^\infty \pm \frac{E_g}{2} \sqrt{1 + \frac{2k_z^2}{m_{\text{eff}}E_g}}. \quad (19)$$

The parameters of the fit given in Fig. 5 are $m_{\text{eff}} = 0.35$, $E_g = 4.0\text{eV}$ and $E_F^\infty = 1\text{eV}$. Our value of the effective mass is to be compared with the electron's mass obtained from DFT calculations for ideal $\alpha\text{-Al}_2\text{O}_3$ crystal, $m_{\text{eff}} \approx 0.4$ ⁴⁷, and fits to experimental $I - V$ characteristics, $m_{\text{eff}} \approx 0.23$ ^{6,48}.

We see that the *sp* model works very well for real as well as imaginary band-structure close to $k = 0$. While both models give the same effective mass, the values of κ for the free-electron like dispersion are larger by $\sim 50\%$ (as indicated by arrows) which contributes to prediction of smaller conductances within the potential barrier model given the interface width is the same, as will be shown in the following section.

VI. THE CONDUCTANCE

Transport properties of the junctions were obtained using the transfer matrix method⁴⁹ implemented in the PWCOND code²³, using plane-wave basis and ultra-soft pseudopotentials. For the given self-consistent Kohn-Sham potential (ob-

code	2L	3L	4L	5L
PWCOND	0.109	0.0166	0.00245	0.000279
WanT	0.0668	0.00730	0.00224	N/A

TABLE II: Values of the conductances in multiples of $e^2/h \times A_z$, where $A_z = 74.23a_B^2$ is the area of the supercell perpendicular to the z direction, calculated by the PWCOND and WanT codes. The differences are similar to the differences between the PWCOND results and the sp model.

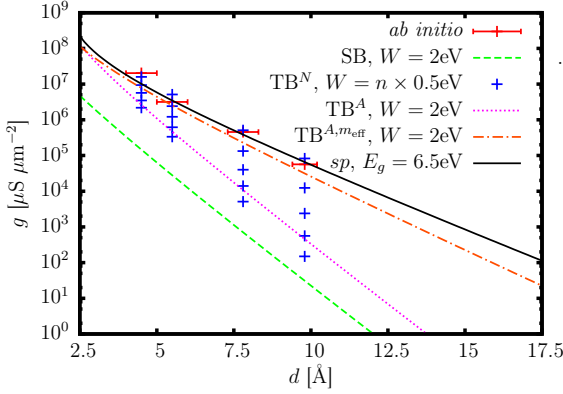


FIG. 6: (Color online) The *ab initio* and model conductances. The square barrier (green dashed line), the trapezoid barrier with transition regions $\Delta d \neq 0$ (pink dotted line) and the inclusion of the effective mass (orange dash-dotted line) form a sequence of improvements of the potential barrier to model towards the true atomic system. Finally, the analytic sp model (black full line) with parameters taken from ground state *ab initio* simulations gives very good agreement with the full first principles calculation of the conductance.

tained from the ground state calculations, see Sec. IV), the conductance was converged with respect to the k_{\parallel} grid; going from the 6×6 mesh (used for the presented results) to a 10×10 mesh the change in the conductance has been found to be $< 5\%$. Furthermore, for testing purposes, the conductances for the 2L, 3L and 4L interfaces were also calculated using the WanT code^{24,25}, where a completely different method based on maximally localized Wannier functions is implemented. Results are reported in Table II and compare well with the previous set, though slightly underestimating the absolute values.

In Figure 6 we show the dependence of the conductances per unit area on the interface width d , determined in Sec. IV, in comparison with the two models considered in Sections II and III. The horizontal error bars accompanying the *ab initio* conductances, $\Delta d \approx 2\text{\AA}$, indicate the width of the transition region between the metal and the insulator, which is taken from the averaged density profile, Fig. 2.

First we consider the potential barrier model with effective mass equal to one, where the calculation of the transmission as well as its energy integration (Eq. 3) are done numerically exactly (TB^N). The potential barrier is of the form given in Fig. 1, where $d_w = d - \Delta d$. The conductances are shown

as the blue crosses, where the height of the energy barrier $W = 0.5neV$, $n = 1, 2, 3, 4, 5$ is increasing from top to bottom. The pink-dotted line is the conductance of the same potential barrier of width $W = 2eV$, but evaluated using the approximate formula [Eq. (6)]. As anticipated in Section II, we see that in view of the overall differences, the approximate but analytic formula is very satisfactory and the numerical calculation of the transmission of its energy integration is not really needed.

We see that in principle, we can achieve agreement between this model and the *ab initio* results if we choose $W \approx 0.5eV$, but this is in stark contrast with the estimates of the potential barrier height from the PDOS, typically taken as the distance between the Fermi energy and the nearest band in the oxide (e.g. the valence band in the oxide in 4L structure according to Fig. 4), here expected to be $W \sim 2eV$.

The green-dashed line is a conductance corresponding to a simple square potential barrier with $W = 2eV$ and effective mass equal to one, and we see that plain square barrier model goes in the wrong direction. The use transition regions of width Δd does shift the potential barrier model in the right direction, particularly for very short interfaces, where the effective mass within the insulator does not seem to play an important role. Hence, use of the transition region between the metal and the insulator of width Δd , given by the spatial extent of the drop if the electronic density between the metal and the oxide, is essential for the TB model.

The red dash-dotted line gives the conductance according to Eq. (6) with the *ab initio* determined effective mass $m_{\text{eff}} = 0.35$ and $W = 2eV$. The effective mass significantly improves the agreement of the potential barrier model with the *ab initio* conductance, while keeping the barrier at the “reasonable” value, motivated by offset between the Fermi energy and the valence band maximum.

Finally, the full black line corresponds to the atomic sp model with the effective mass $m_{\text{eff}} = 0.35$, band gap $E_g = 6.5eV$ and the barrier width $d_w = d - \Delta d$. The use of this reduced width d_w is motivated by two observations: (1) in Sec. II we have seen that the linearly increasing potential at distance Δd contributes to the exponent of the conductance [Eqs. (6-7)] through a much smaller contribution $\Delta d E_F = W/(W + E_F)\Delta d \sim 0.15\Delta d$. (2) in the TB model we have seen that the use of a shorter barrier, effectively given by $d_w + 2/3\Delta d$ [Eq. (7)], is important to compare well with the *ab initio* conductances. Hence we expect that also in the sp model, the oxide width (i.e. the equivalent of the potential barrier) needs to be reduced almost to $d - \Delta d$, which is the value we use. As a result, the sp model is essentially on top of the *ab initio* conductances. While the improvement with respect to the potential barrier model with transition region and the effective mass is not that large, it is important to stress that the parameters of the sp model (E_g , m_{eff} , $d - \Delta d$) correspond to the characteristics of the true *ab initio* model.

It is interesting to attempt a quantitative comparison between experimentally determined barrier widths and heights, and our *ab initio* and sp model results (Fig. 7). As mentioned already in the introduction, there are experimental junctions that are now accessible to first principles simulations. Based on the rather unsatisfactory state of affairs in Fig. 7 we sus-

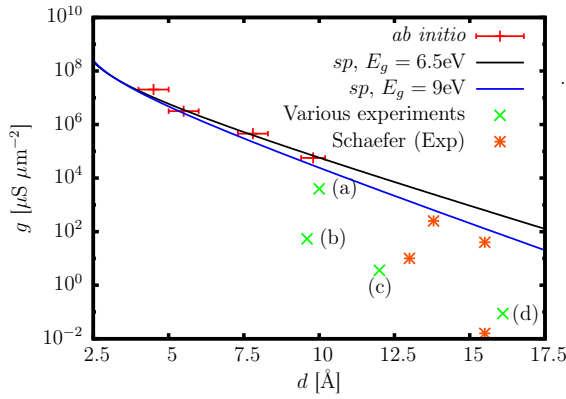


FIG. 7: (Color online) The *ab initio* conductances compared to selected experimental results. (a) Jung¹⁵, (b) Gloos⁸, (c) Holmqvist⁵⁰, (d) Brinkman⁵, and recent experiments by Schaefer⁹. The model gives fairly rigid prediction of the conductances, even using the bandgap of the α -Al₂O₃, $E_g \sim 9$ eV. The likely source of these discrepancies is the experimental determination of the interface width.

pect that not all of the published widths may have been determined correctly. On the other hand, a positive example is the data point taken from the work of Jung¹⁵, where the interface width has been determined directly, and not through fits to the Simmons model and as a result the conductance is relatively closer our *ab initio* conductances. Similar underestimation of the junction widths obtained from Simmons's (potential barrier model) has been obtained in the experimental work of Buchanan *et al.*⁷, even though here it has been interpreted as due to interface roughness.

VII. CONCLUSIONS

In the conclusions, we have analyzed the performance of simple analytical models in describing the conductance of

ultra-thin Al/AIO_x/Al junctions. We have compared atomistic first-principles calculations using the DFT-PBE framework combined with the Landauer formula, with the conductances obtained from a potential barrier and a tight-binding *sp* analytical models. We have shown that the expression for the conductance of the atomic *sp* model has the same form as that from the potential barrier model if the barrier height W is exchanged for $v(E_F)E_g/4$ with $v(E_F) \sim 1$, which explains the small values of W obtained frequently in the past by fitting the potential barrier model to the experimental $I-V$ curves. The accuracy of the analytical models has been tested by using parameters derived from ground-state DFT calculations. We have found that the oxide is characterized by effective mass $m_{\text{eff}} = 0.35$ and bandgap $E_g = 6.5$ eV. When these parameters are used in combination with the *sp* model, excellent agreement with the numerically calculated conductances is found. The interface width used in the models has been shown to correspond to the width of the well-developed oxide which is shorter by about $\Delta d \approx 2$ Å compared to the geometric width of the interface d .

Acknowledgments

This research has been supported by the Slovak Research and Development Agency under the contract No. APVV-0108-11, and the Project HPC-EUROPA++ (RII3-CT-2003-506079). PB would like to thank Kurt Gloos and Hyunsik Im for the correspondence regarding their experimental data. AF acknowledges support from Italian MIUR through Grant No. FIRB-RBFR08FOAL_001.

-
- * Electronic address: peter.bokes@stuba.sk
- ¹ J. C. Fisher and I. Giaever, J. Appl. Phys. **32**, 172 (1961).
 - ² R. Holm, J. Appl. Phys. **22**, 569 (1951).
 - ³ R. Stratton, J. Phys. Chem. Solids **23**, 1177 (1962).
 - ⁴ J. G. Simmons, J. Appl. Phys. **34**, 1793 (1963).
 - ⁵ W. F. Brinkman, R. C. Dynes, and J. M. Rowell, J. Appl. Phys. **41**, 1915 (1970).
 - ⁶ M. Groner, J. Elam, F. Fabreguette, and S. George, Thin Solid Films **413**, 186 (2002).
 - ⁷ J. D. R. Buchanan, T. P. A. Hase, B. K. Tanner, N. D. Hughes, and R. J. Hicken, Appl. Phys. Lett. **81**, 751 (2002).
 - ⁸ K. Gloos, P. J. Koppinen, and J. P. Pekola, J. of Phys. Cond. Matt. **15**, 1733 (2003).
 - ⁹ D. M. Schaefer, P. F. P. Fichtner, M. Carara, L. F. Schelp, and L. S. Dorneles, Journal of Physics D: Applied Physics **44**, 135403 (2011).
 - ¹⁰ C. W. Miller, Z.-P. Li, J. Akerman, and I. K. Schuller, Appl. Phys. Lett. **90**, 043513 (2007).

- ¹¹ V. Lacquaniti, M. Belogolovskii, C. Cassiago, N. D. Leo, M. Fretto, and A. Sosso, New Journal of Physics **14**, 023025 (2012).
- ¹² M. Jonson, Solid State Commun. **33**, 743 (1980).
- ¹³ P. Bokes, Phys. Rev. A **83**, 032104 (2011).
- ¹⁴ P. J. Feibelman, Phys. Rev. B **76**, 235405 (2007).
- ¹⁵ H. Jung, Y. Kim, K. Jung, H. Im, Y. A. Pashkin, O. Astafiev, Y. Nakamura, H. Lee, Y. Miyamoto, and J. S. Tsai, Phys. Rev. B **80**, 125413 (2009).
- ¹⁶ M. M. Fadlallah, C. Schuster, U. Schwingenschlögl, I. Rungger, and U. Eckern, Phys. Rev. B **80**, 235332 (2009).
- ¹⁷ D. Stoeffler, EPL (Europhysics Letters) **59**, 742 (2002).
- ¹⁸ K. D. Belashchenko, E. Y. Tsymbal, I. I. Oleynik, and M. van Schilfgaarde, Phys. Rev. B **71**, 224422 (2005).
- ¹⁹ M. Y. Zhuravlev, R. F. Sabirianov, S. S. Jaswal, and E. Y. Tsymbal, Phys. Rev. Lett. **94**, 246802 (2005).
- ²⁰ W. H. Rippard, A. C. Perrella, F. J. Albert, and R. A. Buhrman, Phys. Rev. Lett. **88**, 046805 (2002).
- ²¹ E. Tan, P. G. Mather, A. C. Perrella, J. C. Read, and R. A.

- Buhrman, Phys. Rev. B **71**, 161401 (2005).
- ²² P. J. Koppinen, L. M. Vaisto, and I. J. Maasilta, Appl. Phys. Lett. **90**, 053503 (2007).
- ²³ A. Smogunov, A. Dal Corso, and E. Tosatti, Phys. Rev. B **70**, 045417 (2004).
- ²⁴ A. Ferretti, A. Calzolari, R. D. Felice, F. Manghi, M. J. Caldas, M. B. Nardelli, and E. Molinari, Phys. Rev. Lett. **94**, 116802 (2005).
- ²⁵ A. Ferretti, A. Calzolari, B. Bonferroni, and R. D. Felice, Journal of Physics: Condensed Matter **19**, 036215 (2007).
- ²⁶ K. H. Gundlach, J. Appl. Phys. **44**, 5005 (1973).
- ²⁷ J. K. Tomfohr and O. F. Sankey, Phys. Rev. B **65**, 245105 (2002).
- ²⁸ E. Prodan and R. Car, Phys. Rev. B **76**, 115102 (2007).
- ²⁹ A. Ferretti, G. Mallia, L. Martin-Samos, G. Bussi, A. Ruini, B. Montanari, and N. M. Harrison, Phys. Rev. B **85**, 235105 (2012).
- ³⁰ M. Mizuguchi, Y. Suzuki, T. Nagahama, and S. Yuasa, Appl. Phys. Lett. **87**, 171909 (2005).
- ³¹ M. S. Chen and D. W. Goodman, J. Phys.: Condens. Matter **20**, 264013 (2008).
- ³² T. Kravchuk, R. Akhvediani, V. V. Gridin, and A. Hoffman, Surf. Sci. **562**, 83 (2004).
- ³³ J. R. Nesbitt and A. F. Hebard, Phys. Rev. B **75**, 195441 (2007).
- ³⁴ A. Hasnaoui, O. Politano, J. M. Salazar, G. Aral, R. K. Kalia, A. Nakano, and P. Vashishta, Surf. Sci. **579**, 47 (2005).
- ³⁵ D. R. Jennison, C. Verdozzi, P. A. Schultz, and M. P. Sears, Phys. Rev. B **59**, R15605 (1999).
- ³⁶ D. Jennison and A. Bogicevic, Surface Science **464**, 108 (2000).
- ³⁷ M. Dieskova, M. Konopka, and P. Bokes, Surf. Science **601**, 4134 (2007).
- ³⁸ P. Giannozzi, S. Baroni, N. Bonini, M. Calandra, R. Car, C. Cavazzoni, D. Ceresoli, G. L. Chiarotti, M. Cococcioni, I. Dabo, A. D. Corso, S. Fabris, G. Fratesi, S. de Gironcoli, R. Gebauer, U. Gerstmann, C. Gougoussis, A. Kokalj, M. Lazzeri, L. Martin-Samos, N. Marzari, F. Mauri, R. Mazzarello, S. Paolini, A. Pasquarello, L. Paulatto, C. Sbraccia, S. Scandolo, G. Sclauzero,
- A. P. Seitsonen, A. Smogunov, P. Umari, and R. M. Wentzcovitch, J. Phys. Condens. Matter **21**, 395502 (2009).
- ³⁹ A. Liebsch, *Electronic Excitations at Metal Surfaces* (Plenum Press, New York, 1997).
- ⁴⁰ L. J. Sham and M. Schluter, Phys. Rev. Lett. **51**, 1888 (1983).
- ⁴¹ R. W. Godby, M. Schluter, and L. J. Sham, Phys. Rev. Lett. **56**, 2415 (1986).
- ⁴² J. P. Perdew and M. Levy, Phys. Rev. Lett. **51**, 1884 (1983).
- ⁴³ N. V. Nguyen, O. A. Kirillov, W. Jiang, W. Wang, J. S. Suhle, P. D. Ye, Y. Xuan, N. Goel, K.-W. Choi, W. Tsai, and S. Sayan, Appl. Phys. Lett. **93**, 082105 (2008).
- ⁴⁴ V. V. Afanas'ev, M. Houssa, A. Stesmans, and M. M. Heyns, J. Appl. Phys. **91**, 3079 (2002).
- ⁴⁵ R. Ahuja, J. M. Osorio-Guillen, J. S. de Almeida, B. Holm, W. Y. Ching, and B. Johansson, Journal of Physics: Condensed Matter **16**, 2891 (2004).
- ⁴⁶ K. Sankaran, G. Pourtois, R. Degraeve, M. B. Zahid, G.-M. Rignane, and J. Van Houdt, Appl. Phys. Lett. **97**, 212906 (2010).
- ⁴⁷ Y.-N. Xu and W. Y. Ching, Phys. Rev. B **43**, 4461 (1991).
- ⁴⁸ S. Ganguly, J. Verma, G. Li, T. Zimmermann, H. Xing, and D. Jena, in *Device Research Conference (DRC), 2011 69th Annual* (IEEE, Santa Barbara, 2011), pp. 121–122.
- ⁴⁹ H. J. Choi and J. Ihm, Phys. Rev. B **59**, 2267 (1999).
- ⁵⁰ T. Holmqvist, M. Meschke, and J. P. Pekola, J. Vac. Sci. Technol. B **26**, 28 (2008).
- ⁵¹ W. Franz, in *Handbuch der Physik*, edited by S. Fluegge (Springer, Berlin, 1956), p. 155.
- ⁵² Throughout the paper we use Hartree atomic units: Energies are in Hartree ($H_a = 27.2\text{eV}$) and lengths in units of the Bohr radius $a_B = 0.529\text{\AA}$.
- ⁵³ In our atomic units, the conductance per unit area is given in units of $e^2 a_B^{-2} / \hbar = 8.69210^{10} \mu\text{S}\mu\text{m}^{-2}$.
- ⁵⁴ The resulting expression is similar to the non-parabolic model discussed by Stratton³ or Gundlach²⁶ and credited to Franz⁵¹.